Materialia 21 (2022) 101365

Contents lists available at ScienceDirect

Materialia

journal homepage: www.elsevier.com/locate/mtla

Full Length Article

Successful prediction of the elastic properties of multiphase high entropy alloys in the AlTiVCr-Si system through a novel computational approach

P. Stavroulakis*, C.L. Freeman, D. Patel, C. Utton, R. Goodall

Department of Materials Science & Engineering, The University of Sheffield, Sir Robert Hadfield Building, Portobello St S1 3JD, Sheffield, UK

ARTICLE INFO

Keywords:
Elastic properties
High entropy alloys
Thermodynamic modelling
Density functional theory
Finite element modelling

ABSTRACT

High-Entropy Alloys (HEAs) are a novel class of materials that can potentially enable novel high-stiffness lightweight alloy design through their exceptional chemical diversity. Most computational techniques for assessing the elastic properties of HEAs are restricted to relatively simple, single phase systems. In this research we present a computational approach capable of assessing the elastic properties of multiphase HEAs and verify it experimentally. Our computational approach involved the combination of several predictive techniques; Thermodynamic Modelling with Thermo-Calc for phase property prediction, Density Functional Theory (DFT) simulations with CASTEP to derive the elastic properties of the phases present in the alloy and Finite Element Modelling (FEM) with ABAQUS to homogenise the elastic properties of each phase into a unified material. The applicability of this methodology is alloy-universal and solely depends on the accuracy of each individual modelling technique used. For verification, the equiatomic AlTiVCr and AlTiVCr-$Si_{7.2}$ high entropy alloys were manufactured through Vacuum Arc Melting (VAM) and were then heat-treated at 1200 °C for 8 h, followed by air-cooling to room temperature. The samples were characterised by Optical and Scanning Electron Microscopy (OM, SEM), X-Ray Diffraction analysis (XRD), together with elastic properties measurements through depth-sensing nanoindentation and microindentation testing. Our approach managed to successfully predict the elastic properties of both materials, yielding a deviation of 10% for the AlTiVCr alloy and only 2% for the AlTiVCr-$Si_{7.2}$ alloy.

1. Introduction

Lowering emissions of greenhouse gases remains a key challenge for transportation [1]. One route to address this is through vehicle weight reduction; however, existing lightweight materials tend to either not satisfy the structural demands of an application or impose an elevated manufacturing (or environmental) cost. One important mechanical property (which is often overlooked in consideration of lightweighting approaches) is the Young's modulus (E) [2]; lightweighting can be a greater challenge with materials possessing low E, as to resist elastic deformation increased component dimensions, and therefore volume and mass, may be needed. As most structural metallic materials have a similar specific stiffness, there is a need for novel alloys which do not exhibit this trend [3]. High Entropy Alloys (HEAs; also known as Complex Concentrated Alloys, CCAs, especially when they exhibit multiphase structures) could prove effective due to their compositional flexibility. The development of high-specific-stiffness multicomponent HEAs is, however, highly complex through a purely experimental approach due to the vast number of potential systems and compositions. Consequently, rapid, accurate and precise computational screening tools are required to guide HEA design.

Density Functional Theory (DFT) has widely been used to predict the elastic properties of single phase metallic alloys and simulate the behaviour of the different incorporated alloying elements [4]. The approach is based on the Hohenberg-Kohn theorem [5] and expressed through the Kohn-Sham equations [6]. This method can only assess cells containing a few tens to hundreds of atoms due to computational limitations. Therefore, the investigation of chemically disordered systems such as HEAs, where it may be difficult to capture a random structure on such a small scale, is particularly difficult without additional approximations. The exact-muffin-tin orbital (EMTO) method [7] was proposed for solving the Kohn-Sham equations alongside a coherent-potential approximation (CPA) to model these systems [8,9]. The drawback of this approach is that it can result in the oversimplification of the investigated system by removing some chemical variation which is not lost with a conventional pseudopotential approach [7]. The review by Huang et al. [10] found the accuracy of the EMTO–CPA method to be comparable to other implementations of DFT. In contrast a comparative investiga-

* Corresponding author.
E-mail address: ppstavroulakis1@sheffield.ac.uk (P. Stavroulakis).

https://doi.org/10.1016/j.mtla.2022.101365
Available online 12 February 2022

tion between experimental data, the Vienna ab initio simulation package (VASP) and the EMTO–CPA implementations of DFT showed that VASP was more accurate than EMTO–CPA in predicting the elastic properties of the CrFeCoNi and CrMnFeCoNi HEAs [11]. This outcome may be different across other HEA systems, or even other DFT implementations, as no in-depth comparative investigations with experimental validation have been carried out. Despite this, both planewave-based and EMTO–CPA implementations of DFT have been widely used to study the elastic properties of various HEA systems, focusing mostly on single phase Body-Centred Cubic (BCC) HEAs [12–16].

The work of Senkov et al. [17,18] on the design of Refractory HEAs (RHEAs) paved the way for lightweight HEA (LWHEA) design via the incorporation of lighter elements in RHEA compositions, aiming to achieve a density reduction while retaining good mechanical performance and preserving their single phase nature [19]. Nevertheless, most alloys developed through this concept are found to exhibit brittle behaviour [20,21] or even decompose into multiple phases during heat treatment [22–24]. Eventually, this led LWHEA research to include the assessment of multiphase systems to enable additional flexibility from a design perspective. Such an alloy design example would be equiatomic AlTiVCr developed by Qiu et al. [25], which was documented to form a single ordered BCC B2 phase through a combination of DFT and atom probe analysis, with a theoretical bulk modulus of 151.6 GPa. This was further supported by a computational study [26] which reported a Young's modulus of the B2 phase over 220 GPa, and a bulk modulus of roughly 150 GPa. This wo'uld produce a specific stiffness greater than even the more advanced high-modulus steels [3] given the low density of the alloy (5.06 g/cm^3 [25]). In 2019, Huang et al. [27] modified the original composition to explore the AlTiVCr-(C/B/Si)$_x$, ($x \leq 5$ at.%) systems and attempted to predict the thermodynamic behaviour through CALPHAD techniques and further increase the mechanical properties. It was observed that these modifications resulted in the formation of secondary phases in most of the examined chemical compositions.

Directly designing and predicting the properties of multiphase HEAs through either planewave-based or EMTO–CPA implementations of DFT is not possible. The *ab-initio* methods use simulation cells comprised of only a few thousand atoms at most. Therefore, the applicability and accuracy of such computational techniques for HEAs is restricted to relatively simple, single phase systems. Consequently, a computational approach capable of assessing the elastic properties of multiphase materials is required.

In this research we present a novel computational methodology for alloy screening by calculating the elastic properties of multiphase HEAs, and show its experimental verification with the equiatomic AlTiVCr and AlTiVCr-Si$_{7.2}$ high entropy alloys, assessing these for their structure and elastic properties. The elastic properties of the investigated materials were extracted computationally and were subsequently verified by comparison with results obtained using experimental methods. Therefore, in order to provide a suitable test of the modelling approach, no experimental results were used to inform computational aspects of the investigation and no computational findings were used to aid in the experimental assessment of these materials.

2. Methods

As previously mentioned, the equiatomic AlTiVCr and the AlTiVCr-Si$_{7.2}$ were chosen for this investigation. That was because the addition of Si would enable the formation of Ti_5Si_3 and thus allow us to test our approach on both a single phase and dual phase material. An increased Si content allowed us to further approach a eutectic composition, as suggested in the work of Huang et al. [27], and as such increase the volume fraction of the Ti_5Si_3 phase, simplifying the characterisation process.

2.1. Modelling methods

Our general approach is to combine different modelling methods, each of which addresses a part of the problem.

- Thermodynamic Modelling with Thermo-Calc Software for the prediction of the equilibrium phases present in our alloys and their volume ratios.
- Density Functional Theory (DFT) simulations with CASTEP to assess the stability of candidate phases and derive the elastic properties of each phase.
- Finite Element Modelling (FEM) with ABAQUS to homogenise the elastic properties of each phase into a unified material.

The overall accuracy of the approach depends on the accuracy of each individual computational technique. Therefore, where required, the substitution of each technique with more accurate counterparts is an option, depending on the availability of computational resources and required databases.

2.1.1. Thermodynamic simulations – thermo-calc software

The Thermodynamic calculations were carried out using the commercial software Thermo-Calc 2 version 2020a using SSOL4: SGTE Alloy Solutions Database v.4.9.g [28]. The phase volume fraction and matrix composition calculations were performed for 7.2 at.% Si at 800 °C. According to the computational results, 800 °C would roughly be the temperature where the solubility of Si in the matrix phase nears a minimum and is predicted to have precipitated in the form of Ti_5Si_3 particles at this temperature. Although the material has been heat-treated at 1200 °C during the experimental assessment, that does not guarantee that no additional formation of the Ti_5Si_3 took place during the air cooling process as more Si becomes available with a reduction in temperature. Further information regarding the thermodynamic simulations is provided in the supplementary material.

2.1.2. Density functional theory calculations - CASTEP

The DFT calculations investigated the matrix phases of the two HEAs and the Ti_5Si_3 intermetallic phase using CASTEP, a first-principles-derived code for electronic structure calculations, capable of approximating the exchange-correlation functional [29]. The software uses a planewave-based pseudopotential approach to solve a set of one-electron Kohn-Sham equations [30].

A $2 \times 2 \times 2$ Body Centred Cubic (BCC) supercell containing a total of 16 atoms was used for the calculations regarding the matrix phase of the AlTiVCr and AlTiVCr-Si$_{7.2}$ alloys. In the first case the supercell contained an equiatomic ratio of alloying elements, while in the latter the tested composition contained 25 at.% Al, 12.5 at.% Ti and 31.25 at.% V and Cr, respectively. This was to reflect the reduction of the Ti content in the matrix phase as a significant amount of Ti is utilised in the formation of the Ti_5Si_3 phase in the AlTiVCr-Si7.2 alloy as captured by Thermo-Calc. Ten different AlTiVCr supercells, each with a unique random arrangement of the atoms on the lattice sites were created for each matrix phase and tested in relation to their total energy to ensure that an energetic equivalency is evident between all configurations. From these configurations, three were randomly selected for the subsequent elastic property calculations. A $2 \times 2 \times 2$ Hexagonal Close-Packed (HCP) supercell was used for the Ti_5Si_3 calculations, also containing 16 atoms.

The electron-electron interactions were approximated using the Perdew, Burke Erzenhof (PBE) exchange-correlation functional [31]. Ultrasoft pseudopotentials were used for both the AlTiVCr and Ti_5Si_3 simulations. For the electronic minimisation routine, the Pulay density mixing method [32] was selected and the SCF cycle energetic tolerance was defined at 5×10^{-7} eV. A Gaussian smearing scheme [33] with a smearing width of 300 K using 48 additional bands was used to simulate a higher temperature environment and allow for proper K-point distribution. The geometry optimisation process was executed using the limited-memory Broyden-Fletcher-Goldfarb-Shanno (LBFGS) algorithm [34]. To achieve good precision in the geometry optimisation routine, a 750 eV and 700 eV cutoff energy was selected for the AlTiVCr-based and Ti_5Si_3 supercells respectively along with 0.014 Monkhorst-Pack [35] grid spacing and a finite basis correction of 5 eV over three steps. Symmetry operations were enabled to speed up the calculation, while the supercell

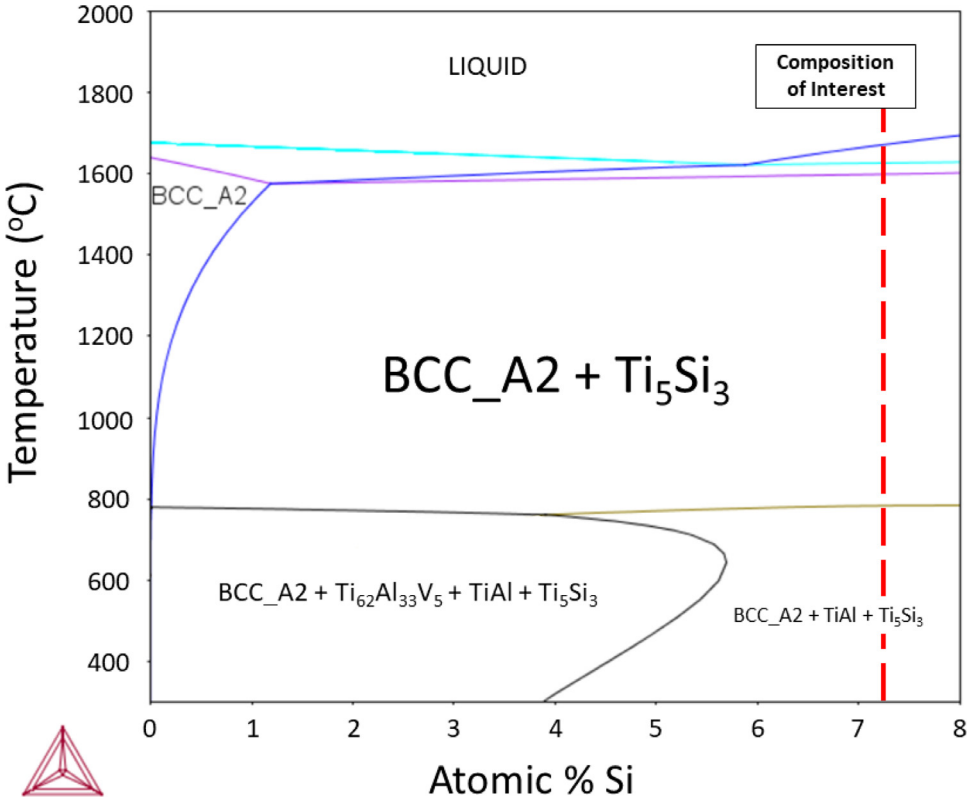

Fig. 1. Calculated phase diagram of the AlTiVCr-Si_x system with Thermo-Calc Software using the SSOL4: SGTE Alloy Solutions database. The composition of the alloy with the silicon addition studied here is indicated.

was forced to maintain symmetry during optimisation when possible. Convergence was achieved in respect to the final stress tensor of all investigated supercells up to 10 MPa per stress component.

Full geometry optimisations were performed where the atoms could relax to their lowest energy state with variation of the lattice parameters and ionic movement while the centre of mass was constrained. For the AlTiVCr-based supercells, the initial energy, force, stress, and displacement tolerances were specified at 2.5×10^{-5} eV, 4×10^{-2} eV/ Å, 4×10^{-2} GPa and 2.5×10^{-3} Å, respectively. For the Ti_5Si_3 supercell, the initial energy, force, stress, and displacement tolerances were specified at 5×10^{-5} eV, 10^{-2} eV/ Å, 5×10^{-3} GPa and 5×10^{-3} Å. Once the geometrically optimised structures were generated, we applied a set of deformations as described in [7] depending on the crystal structure of each phase and performed a secondary geometry optimisation using the same convergence criteria with a constrained cell size while permitting ionic movement. The elastic constants for each single crystal were extracted through fitting the stress tensor calculated through CASTEP to the strain applied from the deformation patterns. Lastly, the polycrystalline (isotropic) elastic properties of each phase were calculated according to the guidelines provided in [36,37] using the Voigt-Reuss-Hill (VRH) approximation.

2.1.3. Homogenisation modelling

A homogenisation modelling approach was used to combine the elastic properties of the Ti_5Si_3 intermetallic phase with that of the matrix phase of the AlTiVCr-$Si_{7.2}$ alloy, as calculated through DFT. We used the commercial software ABAQUS along with the Micromechanics plugin for the creation of a representative volume element (RVE) and the EasyPBC plugin [38] to perform the homogenisation. The employed homogenisation scheme is a combination of the RVE method and the Asymptotic Homogenisation (AH) approach [39]. The RVE was designed to include a Ti_5Si_3 ellipsoid with homogenized elastic properties according to the VRH approximation. The matrix phase was also informed using the VRH approximation in terms of its elastic properties.

2.2. Experimental methods

2.2.1. Materials and processing

The raw materials used to manufacture the alloy (Al pieces and sheets, Cr pieces, 1 mm Si lumps, Ti wires and rods, V turnings) with purities >99.8% were supplied by NewMet Ltd, Waltham Abbey, UK. Experimental samples in the shape of ellipsoids with a diameter of 25 mm and 10 mm thickness were formed using an Arcast Arc 200 Vacuum Arc Melter (VAM) under a high purity argon (Ar) gas atmosphere and remelted 4–5 times to ensure chemical homogeneity. One AlTiVCr and AlTiVCr-$Si_{7.2}$ sample were sectioned, and one half of each sample was used for metallographic preparation while the other half was heat-treated. The heat-treatment was carried out in a laboratory electric furnace under a flowing Ar atmosphere, along with two Ti pieces for each half to act as an oxygen getter and ensure minimal oxidation, at 1200 °C for 8 h. Density data were extracted using Archimedes' method. The samples were mounted in conductive bakelite and were ground using P120, P280, P600, P1000, P1200, P2500 and P4000 SiC grinding papers in succession. They were then polished using a 1 μm diamond suspension and Struers OP-U colloidal silica solution for 10 and 20 min respectively for relief polishing.

2.2.2. Optical (OM), scanning electron (SEM) microscopy & electron dispersive X-ray spectroscopy (EDS)

The microstructures of the samples were investigated using a Nikon Eclipse LV150 Optical Microscope (OM) under polarised light, using the analyser and darkfield filters. Further microstructural and fracture surface investigation was carried out using a FEI XL30 S Field Emission Gun Scanning Electron Microscope (SEM) with Secondary (SE) and Backscatter Electrons (BSE) under 20 kV accelerated voltage, in conjunction with Energy-Dispersive X-Ray Spectroscopy Analysis (EDS) to evaluate possible segregation phenomena and perform phase analysis and characterisation.

Table 1
Predicted chemical composition of the AlTiVCr-$Si_{7.2}$ alloy matrix phase at 800 °C compared to the experimentally measured heat-treated matrix composition.

Elements	Nominal Composition (at.%)	Experimental Matrix Composition (at.%)	Predicted Matrix Composition (at.%) (using SSOL4)
Al	23.2	27.78	28.70
Ti	23.2	18.78	13.86
V	23.2	25.59	28.70
Cr	23.2	26.87	28.70
Si	7.2	0.98	0.040

Table 2
Mean calculated elastic constants of the AlTiVCr and AlTiVCr-$Si_{7.2}$ alloy matrix phases.

	Elastic Constants (GPa)		
Alloy Matrix Phase	C_{11}	C_{12}	C_{44}
AlTiVCr	208.5 ± 18.9	116.4 ± 12.8	82.0 ± 11.0
AlTiVCr-$Si_{7.2}$	245.0 ± 1.9	127.7 ± 3.0	84.5 ± 4.9

2.2.3. X-ray diffraction analysis

For the determination of crystal structure of the bulk alloys, in both the as-cast and heat-treated conditions, X-ray Diffraction (XRD) was carried out using a Bruker D2 Phaser diffractometer with N K-β filtered Cu Kα radiation operating at 30 kV and 10 mA. The upper and lower discriminators were 0.11 and 0.25 V respectively. The scanning angle range was set from 20° to 80° 2θ with a step size of 0.02° and with the sample rotating at 15 rpm. For the as-cast AlTiVCr, as-cast AlTiVCr-Si7.2 and heat-treated AlTiVCr-Si7.2 a 0.2 mm primary divergence slit was used while for the heat-treated AlTiVCr a 1 mm primary divergence slit was used instead. Subsequent phase analysis was undertaken using the International Centre for Diffraction Data's (ICDD) PDF-4+ database (2022 edition) and the associated SIeve+ software.

2.2.4. Indentation testing (nano/micro)

For the evaluation of the elastic properties of the tested materials, the nanoindentation and microindentation testing techniques were employed, using a Hysitron Ti Premier nanoindenter and a MicroMaterials NanoTest microindenter respectively. In both cases, standard Berkovich tips were used with a load function consisting of 5 s load, 5 s dwell and 5 s unload times. The tests were load controlled and were limited to a maximum load of 3000 μN and 300 mN for the nanoindentation and microindentation, respectively. The nanoindentation grids used were 10 × 10 with a 10 μm spacing for all samples. The microindentation grids used were a 5 × 5 grid with 100 μm spacing for the as-cast AlTiVCr sample, a 10 × 10 grid with 100 μm spacing for the heat-treated AlTiVCr sample, a 10 × 20 grid with 250 μm spacing for the as-cast

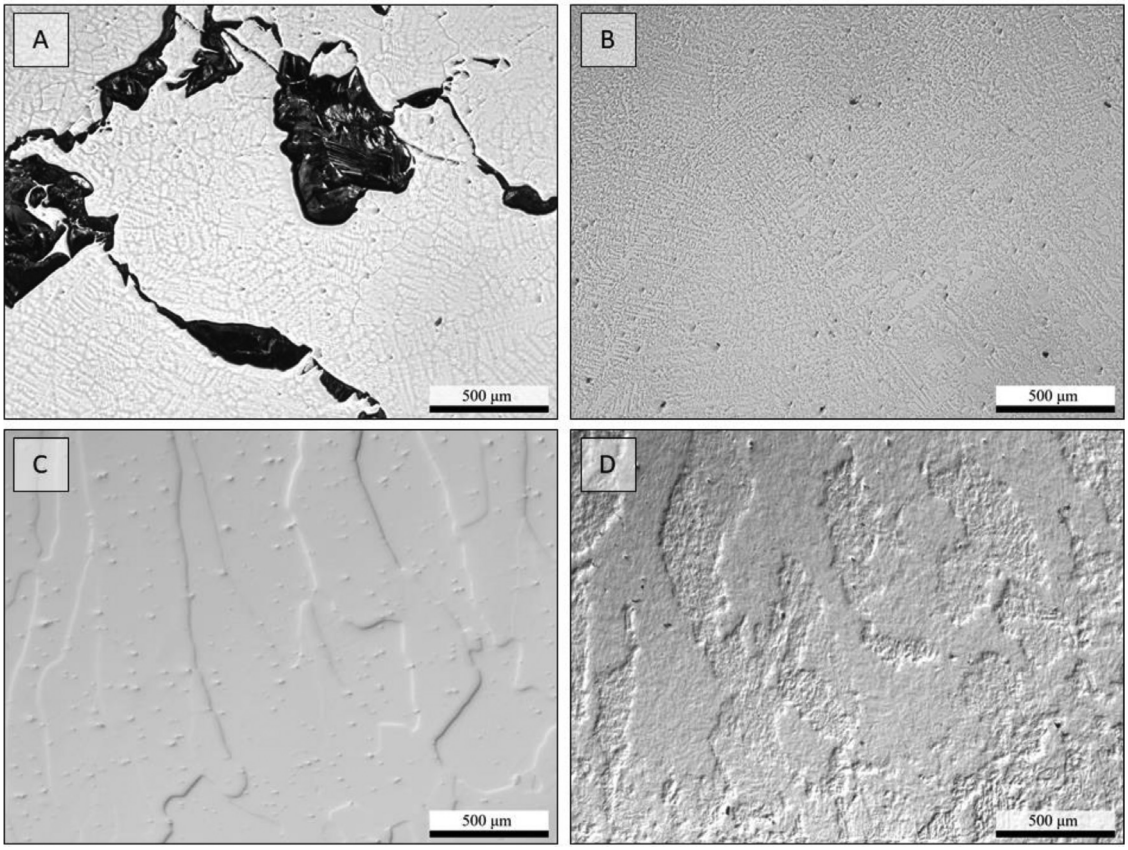

Fig. 2. Optical micrographs at x50 magnification of relief polished specimens from the central region of the A) as-cast AlTiVCr, B) as-cast AlTiVCr-$Si_{7.2}$, C) heat-treated AlTiVCr and D) heat-treated AlTiVCr-$Si_{7.2}$ samples.

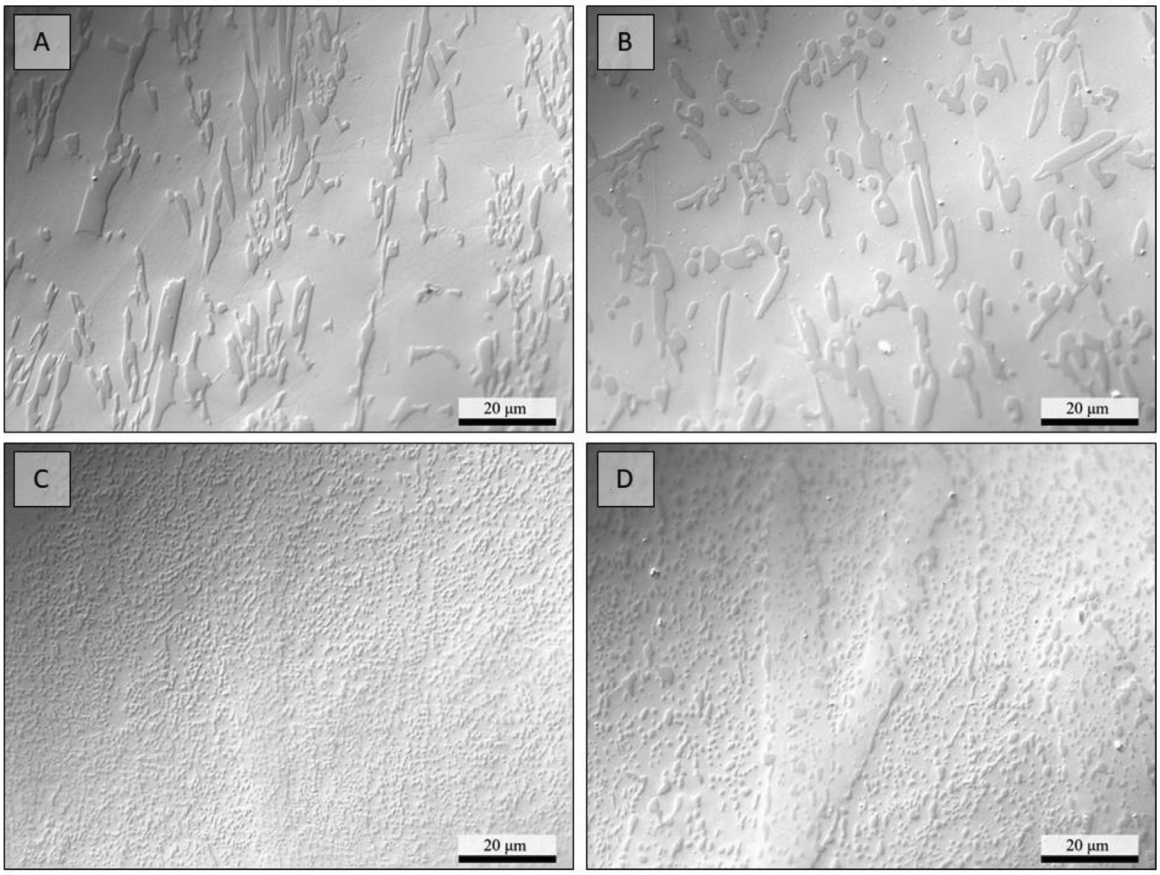

Fig. 3. Optical micrographs at x1000 magnification relief polished specimens of the central region of the A) as-cast AlTiVCr-$Si_{7.2}$, B) heat-treated AlTiVCr-$Si_{7.2}$ and the surface (high cooling rate) region of the C) as-cast AlTiVCr-$Si_{7.2}$, D) heat-treated AlTiVCr-$Si_{7.2}$ samples.

AlTiVCr-$Si_{7.2}$ sample and a 10 × 10 grid with 100 μm spacing for the heat-treated AlTiVCr-$Si_{7.2}$ sample.

2.3. Error calculation

All errors presented in this work are expressed as the standard deviation in the data. Information regarding the number of data points is included within each individual methods section where relevant.

3. Results and discussion

3.1. Modelling predictions

3.1.1. Phase prediction and analysis

The first step of our methodology depends on achieving an adequate thermodynamic description of the system of interest. Thus, it is important to evaluate the capability of thermodynamic databases in terms of phase prediction and fraction analysis for the HEA system. A similar study, concerning the same alloys, in the AlTiVCr system was carried out by Huang et al. [27], where the TCHEA2: TCS High Entropy Alloys Database was used. Their work showed the formation of a single ordered Body-Centred-Cubic (BCC) B2 phase when assessing the equiatomic AlTiVCr alloy without Si addition, below 700–900 °C. They also suggested the initiation of an order-disorder transformation taking place at that temperature.

In this work we are instead using the SSOL4 thermodynamic database. There are limitations to using the SSOL4 database for these systems, as we know it cannot predict the order to disorder transformation for these alloys (see supplementary information). Our calculations (Fig. 1) indicated that the formation of the ALM_DO19 ($Ti_{62}Al_{33}V_5$) and TiAl phases is instead favoured below the temperature threshold, alongside a disordered BCC phase. The stability of the B2 phase at lower temperatures has been previously verified in the work by Qiu et al. [25] both experimentally and computationally, while no evidence was found for the formation of the TiAl and ALM_DO19 phases. However, their experimental investigation only focussed on rapidly cooled as-cast samples.

With the addition of Si, both databases predicted the presence of the Ti_5Si_3 phase for the entire solid-state temperature range. Additionally, our study suggested that for a lower Si content the TiAl and ALM_DO19 SPPs form alongside the Ti_5Si_3 phase, while for a greater Si content the ALM_DO19 phase is no longer evident.

The prediction of these phases at lower temperatures suggests that either the SSOL4 database is not accurate enough in terms of phase prediction in the present HEA system (in contrast to the TCHEA2 database used by Huang et al. [27]) or that the kinetics of formation for the secondary phase particles (SPPs) are relatively sluggish, and thus would require a low-temperature heat-treatment of extensive duration for their precipitation to occur. As far as the authors are aware, no experimental research has been carried out to date to investigate a lower temperature thermodynamic equilibrium where these transformations are indicated to occur in the present system.

It is once again underlined that the current database is unable to predict this order-disorder transformation and as such the results concerning temperatures under 800 °C would be considered questionable. Nevertheless, as the temperature spectrum of interest in this work lies within the dual phase BCC_A2 – Ti_5Si_3 region roughly above 800 °C (Fig. 1), it was decided that the current thermodynamic predictions using SSOL4 were sufficient for the present study. The expected volume fraction of the Ti_5Si_3 particles in the AlTiVCr-$Si_{7.2}$ alloy was calculated here at approximately 20%. Another phenomenon predicted in the present study

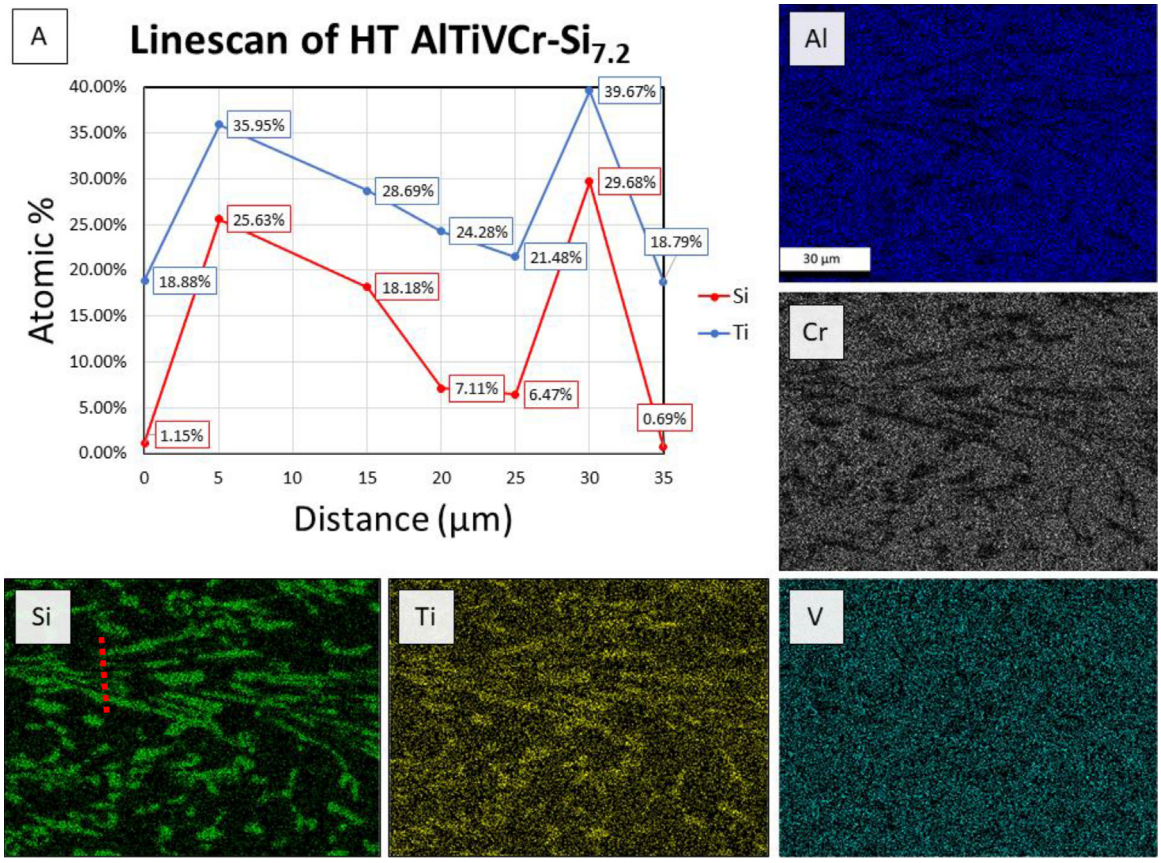

Fig. 4. Investigation of the heat-treated AlTiVCr-$Si_{7.2}$ alloy showing: A) The Si and Ti content along a linescan where increases in both elements suggest the presence of Ti_5Si_3 intermetallics within an AlTiVCr matrix, and the distribution of Al, Ti, V, Cr and Si content in the present sample. Linescan path indicated with a red dotted line on the Si quant map image. (For interpretation of the references to color in this figure legend, the reader is referred to the web version of this article.)

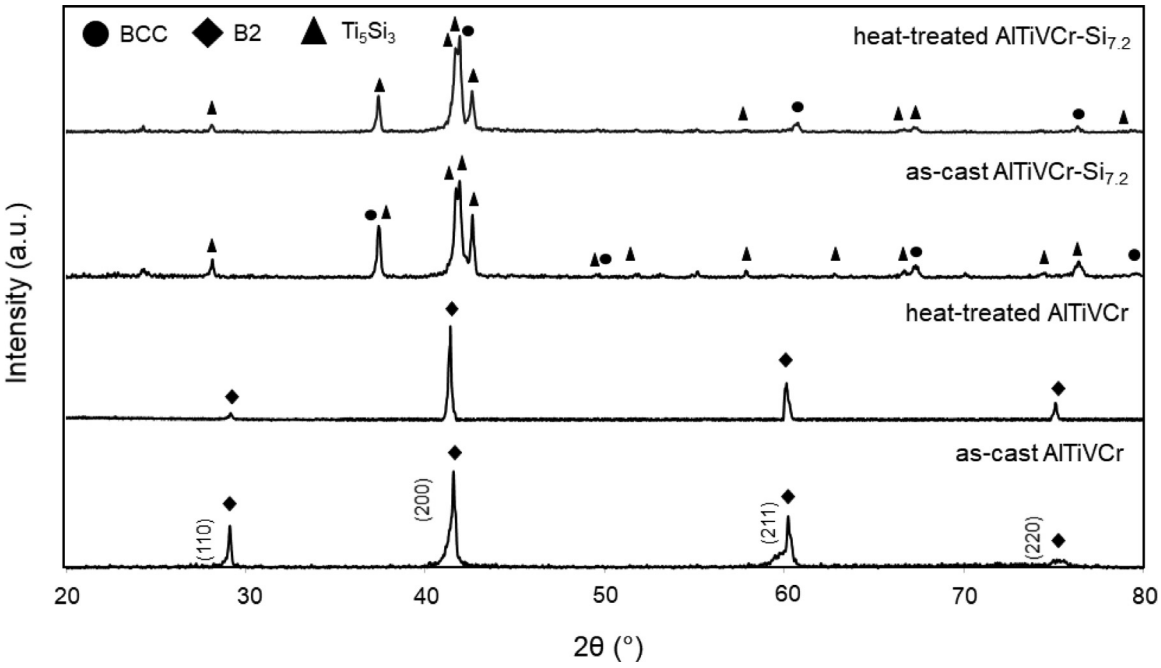

Fig. 5. Normalised XRD patterns of the as-cast and heat-treated AlTiVCr and AlTiVCr-$Si_{7.2}$ alloys.

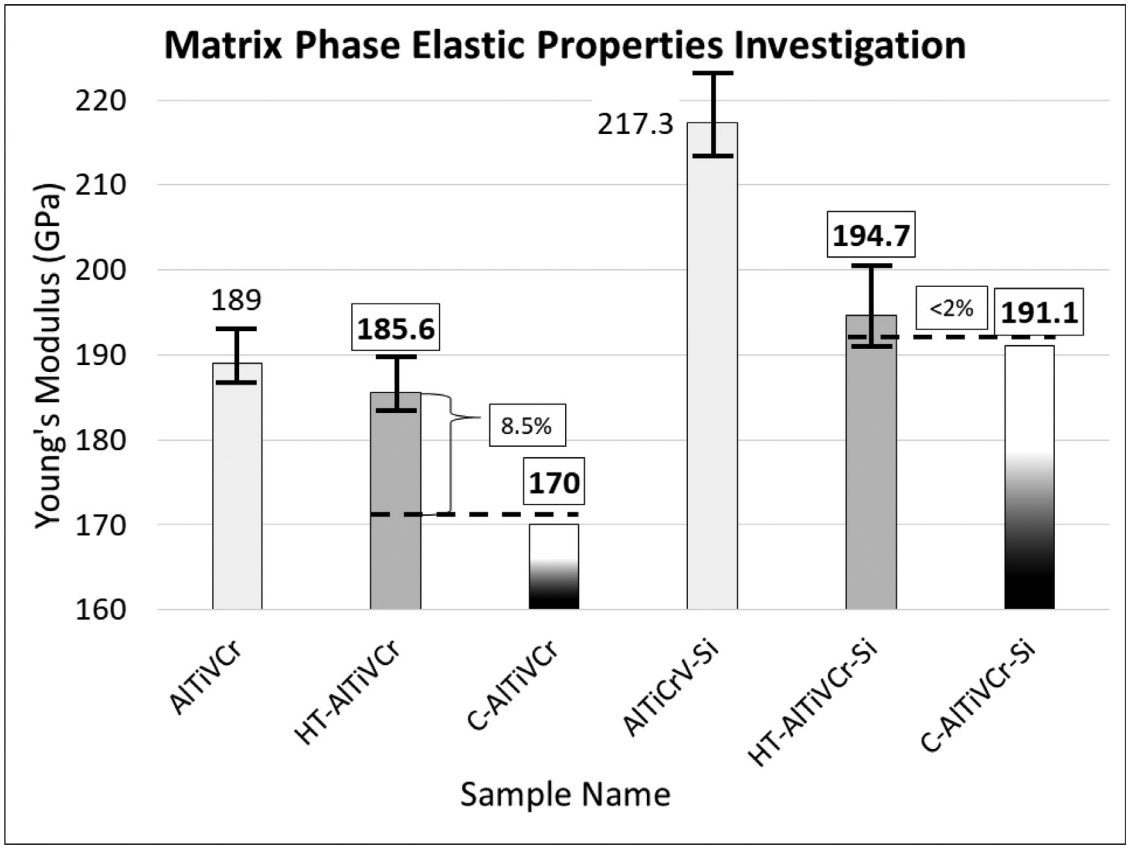

Fig. 6. Nanoindentation Young's modulus of the matrix phases of the AlTiVCr, heat-treated (HT)-AlTiVCr, AlTiVCr-$Si_{7.2}$, HT-AlTiVCr-$Si_{7.2}$ alloys compared to the ones derived computationally (C) through CASTEP.

is the depletion of the AlTiVCr matrix in both Ti and Si. This occurs as both alloying elements are involved in the formation of the Ti_5Si_3 secondary phase (Table 1).

3.1.2. Elastic properties

Based on the thermodynamic calculations, we now know that the AlTiVCr alloy is composed of a single BCC matrix phase and that the AlTiVCr-$Si_{7.2}$ alloy has a dual phase microstructure containing a BCC matrix phase, which is reduced in Ti content, and the Ti_5Si_3 intermetallic phase. To proceed with the prediction of the alloy properties we firstly assess each phase individually in terms of their elastic properties, initially through computational means, followed by experimental validation. The CASTEP simulations predicted a lattice parameter of 3.053 Å for the AlTiVCr alloy, which compares well to the experimental values of 3.075 Å [25], and 3.008 Å for the matrix phase of the AlTiVCr-$Si_{7.2}$ alloy.

The mean calculated C_{11}, C_{12} and C_{44} components of the elastic tensor of the AlTiVCr and the matrix phase of the AlTiVCr-$Si_{7.2}$ alloys are shown in Table 2. The mean bulk modulus (B) of the AlTiVCr alloy was estimated at 147.1 GPa which agrees with the previously computationally reported value of 146.6 GPa for the BCC lattice [25]. Additionally, our estimates for the shear modulus (G) indicated a mean modulus of 65.0 GPa. Lastly, from B and G the Young's modulus (E) and Poisson's ratio (v) were estimated at 170.1 GPa and 0.31, respectively. As for the AlTiVCr-$Si_{7.2}$ matrix, our computational calculations produced a mean bulk modulus (B) of 166.8 GPa and a shear modulus (G) of 73.0 GPa, while the Young's modulus (E) and Poisson's ratio (ν) were estimated at 191.2 GPa and 0.31 respectively.

Regarding the Ti_5Si_3 intermetallic phase, the results of our simulations deviated from the reported elastic constants C_{11}, C_{12}, C_{13}, C_{33}, C_{44} and C_{66} found in other computational work [40,41] by up to 25%. Our estimates for the bulk and shear moduli stood at 141.8 GPa and 96.6 GPa respectively while the reported values were 139 GPa and 94 GPa respectively. The Young's modulus and the Poisson's ratio were estimated to be 236.1 GPa and 0.22 in our work while the previously reported computationally-derived values were 231.3 GPa and 0.22, respectively. However, as the deviation of our computational and experimental result for the bulk, shear and Young's moduli is less than 3%, our estimate is deemed satisfactory.

3.1.3. Material homogenisation

All the collected information on the phases present in the AlTiVCr-$Si_{7.2}$ alloy and their elastic properties are used in ABAQUS and homogenised into a unified material. The homogenised computational Young's modulus was estimated at 200.1 GPa with a Poisson's ratio of 0.29.

3.2. Experimental verification and analysis

3.2.1. Microstructure characterisation

Our experimental investigation of the as-cast and heat-treated conditions of the equiatomic AlTiVCr alloy through OM and SEM also showed no evidence of any secondary phases having formed (Figs. 2 and 3). Shrinkage porosity was notable especially in the case of the AlTiVCr sample where cracks were found propagating from one porous region to another. Nevertheless, fine pores were also present in both materials within the interior regions without any indication of cracks. Experimental validation through OM and SEM showed that the Ti_5Si_3 phase was indeed present in both the as-cast and heat-treated conditions of the AlTiVCr-$Si_{7.2}$ alloy, with no sign of any other SPPs (Figs. 2–4). The volume fraction of the Ti_5Si_3 particles was measured as 23% and 24% in the as-cast and heat-treated condition respectively. The distribution of

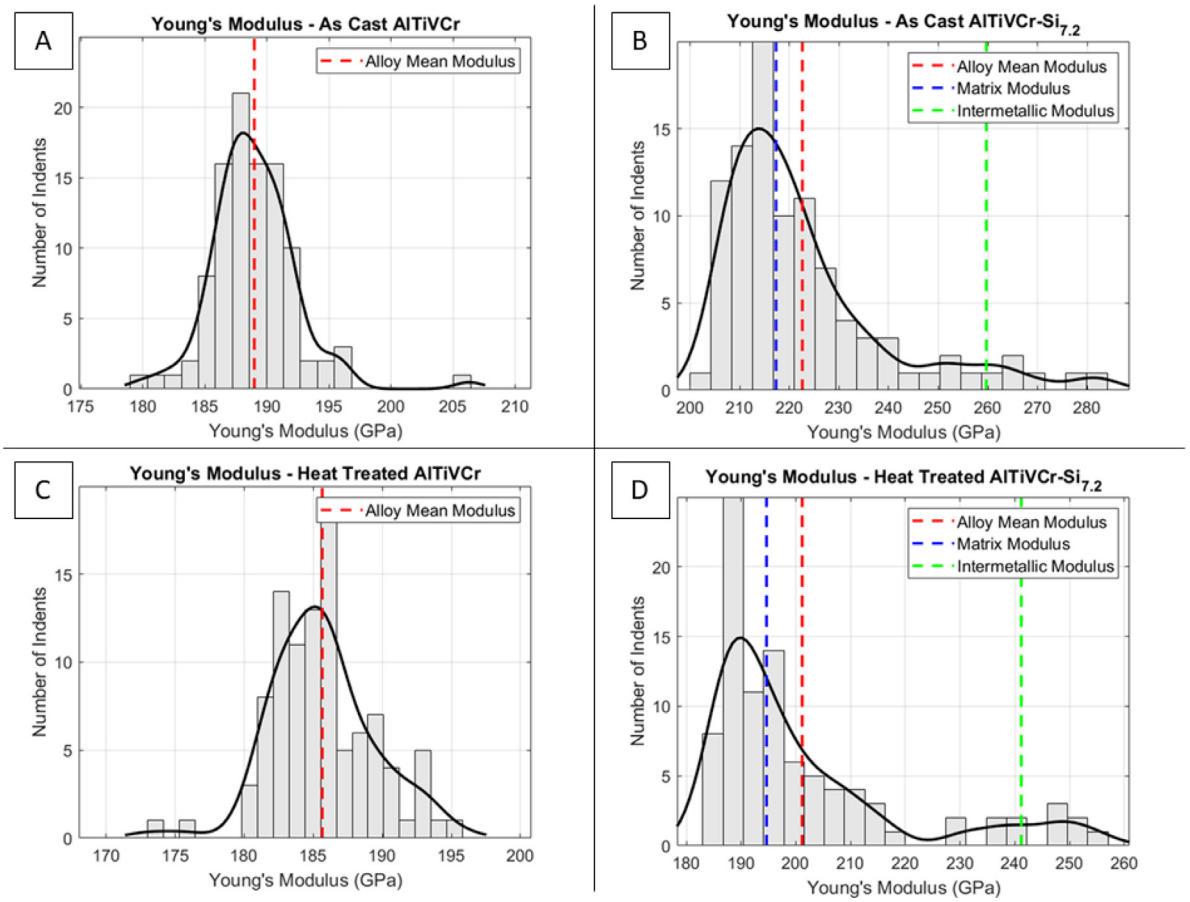

Fig. 7. Nanoindentation measurements of the matrix phase, intermetallic phase and mean alloy Young's moduli of the A) as-cast AlTiVCr, B) as-cast AlTiVCr-$Si_{7.2}$, C) heat-treated AlTiVCr and D) heat-treated AlTiVCr-$Si_{7.2}$ samples.

the Ti_5Si_3 particles in the AlTiVCr matrix was relatively homogeneous without preferential formation points, while the intermetallics' size and shape varied significantly depending on the local cooling rates, as seen in Figs. 2 and 3. This resulted in the production of coarse, elongated intermetallics near the centre and very fine spherical particles near the surface of the samples, where the cooling rate was highest. During the heat treatment, the intermetallics in the central region appeared to undergo a fragmentation and partial spheroidisation process. The particles closer to the surface, however, seemed to undergo an agglomeration process, hinting at an Ostwald ripening mechanism. This suggestion is further strengthened by the fact that the apparent number of particles per unit area in the heat-treated condition is significantly reduced in comparison to that of the as-cast condition. In turn, this observation points to the dissolution of some (likely the smaller) particles and the migration of their constituent alloying elements towards other (likely coarser) particles, resulting in the growth of the latter. Furthermore, the dendrites evident in both as-cast samples were erased during the heat treatment, supporting the assumption that a temperature of 1200 °C is sufficient to enable extensive diffusion to take place in the duration of the heat treatment. Lastly, no significant grain growth was observed between the as-cast and heat-treated conditions of either sample.

Both the quantitative analysis of the alloying elements present in the matrix phase of the AlTiVCr-$Si_{7.2}$ produced using Thermo-Calc software with SSOL4 and the EDS analysis (Fig. 4) point to a degree of Ti and Si depletion in the matrix phase. This effect is not, however, as significant as predicted using Thermo-Calc software with SSOL4 (Table 1). In turn, this leads to an effective change in the ratio of the alloying elements in the matrix, deviating from an equiatomic composition. This indirect compositional tuning may have elevated the elastic properties of the matrix phase. Overall, most of the phenomena that were experimentally verified to occur in the investigated systems were qualitatively captured by thermodynamic modelling with the SSOL4 database; this is an acceptable degree of precision for use as a basis for our subsequent calculations. In conclusion, the thermodynamic simulations showed that the SSOL4 database can provide an adequate description of the behaviour of the AlTiVCr and AlTiVCr-$Si_{7.2}$ alloys concerning the high-temperature (above 800 °C) region. However, there are some points of disagreement with the TCHEA2 database regarding temperatures under 800 °C as SSOL4 is unable to predict the order-disorder transformation.

3.2.2. *X-ray diffraction analysis (XRD)*

Fig. 5 shows the normalised experimental XRD patterns for the high entropy alloys: as-cast and heat-treated AlTiVCr and as-cast and heat-treated AlTiVCr-$Si_{7.2}$. The as-cast AlTiVCr pattern was indexed to a single ordered BCC B2 phase analogous to a $CuNiTi_2$ structure with a space group Pm-3 m (221) and lattice parameter $a \approx 3.05$ Å [42]. The heat-treated AlTiVCr pattern was also indexed to a single B2 phase and is analogous to that identified in the as-cast condition. As such, it is likely that AlTiVCr forms a single ordered B2 matrix as the XRD pattern presents an ideal match to that of structures known to be B2. The as-cast AlTiVCr-$Si_{7.2}$ pattern was indexed to a BCC phase and an HCP phase. The BCC phase is analogous to a $U_{0.65}Pu_{0.13}Mo_{0.22}$ structure with a space group Im-3 m (229) and a lattice parameter $a \approx 3.05$ Å [43]. The heat-treated AlTiVCr-$Si_{7.2}$ pattern was also similarly indexed to a BCC phase and an HCP phase. The BCC phase is analogous to a $Ti_{0.65}Fe_{0.35}$ structure with a space group Im-3 m (229) and a lattice parameter $a \approx 3.06$ Å [44]. Nevertheless, it is not possible to clearly discern a BCC from a B2 crystal structure purely from XRD data, especially when the lattice pa-

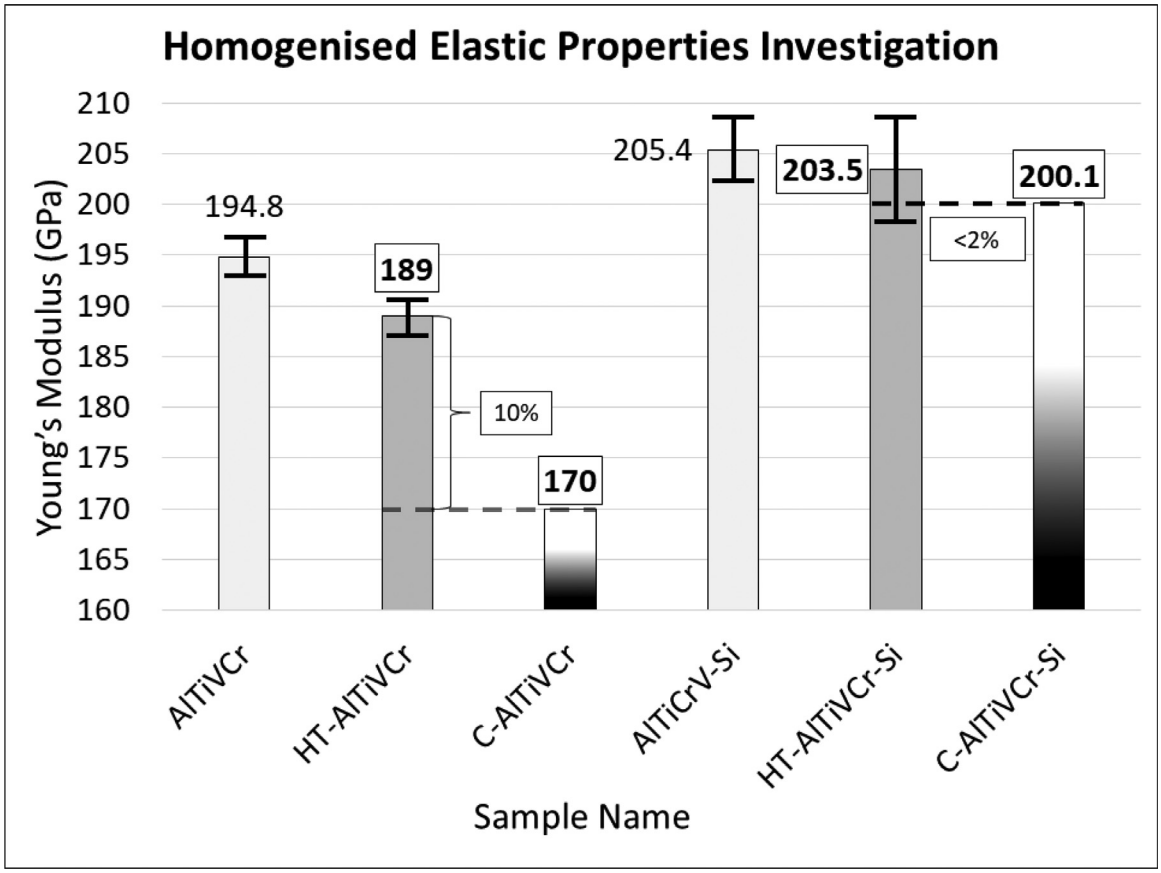

Fig. 8. Microindentation Young's modulus of the AlTiVCr, heat-treated (HT)-AlTiVCr, AlTiVCr-$Si_{7.2}$, HT-AlTiVCr-$Si_{7.2}$ alloys compared to the computationally (C) derived ones through CASTEP and ABAQUS.

rameters of the two are similar as in the present case [25]. This matter would require additional experimentation which is past the scope of this work. Regardless, no distinct changes in the crystal structure between the as-cast and heat-treated conditions are evident. The HCP phase is analogous to a Ti_5Si_3 structure with a space group P63/mcm (193) and a lattice parameter $a \approx 7.43$ Å and $c \approx 5.14$ Å [45]. The HCP phase in the heat-treated sample is analogous to that identified in the as-cast condition. Therefore, it is clear that the Ti-Si intermetallic phase identified during the SEM investigation is indeed the Ti_5Si_3.

Compared to the work by Qiu et al. [25] the XRD patterns of the AlTiVCr samples presented within our research are shifted by a few degrees. This could be attributed to the different sample preparation routes used in the two studies, as a powdered sample was used in their study. Furthermore, the as-cast AlTiVCr and AlTiVCr-$Si_{7.2}$ samples display broader Bragg's peaks compared to their heat-treated counterparts which is attributed to the elimination of pre-existing segregation phenomena through the heat-treatment.

3.2.3. Elastic properties

The as-cast condition of the AlTiVCr alloy was measured as having a Young's modulus of 194.8 ± 3.7 GPa and 189.0 ± 3.4 GPa through means of microindentation and nanoindentation, respectively. Measurements on the homogenised alloy with microindentation and nanoidentation also pointed at a Young's modulus of 189.0 ± 3.7 GPa and 185.6 ± 3.7 GPa, showing no significant indentation size effects. Our computational estimates of the Young's modulus of the phases individually therefore only deviated by about 10% from the experimentally measured value, with microindentation recording 189.0 GPa in the heat-treated condition. Our experimental results contrast with those presented in previous computational research by Huang et al. [26], where a significant difference in the Young's modulus between the ordered and disordered BCC phase was found. The main differences between the computational aspects of the two studies were using the disordered BCC phase for our calculations, and the use of a different quantum-mechanical approach in their case with the EMTO–CPA method. For most alloy development requirements, where modelling would be looked to for an indication of properties, and would be followed up with experimental processing, the level of agreement (up to 10% deviation) we observe between the computational and experimental results would be satisfactory (Fig. 6).

When assessing the AlTiVCr-$Si_{7.2}$ alloy experimentally, the nanoindentation measurements indicated that two groups of results are observed, which are likely to correspond to indents which primarily fall within either the Ti_5Si_3 intermetallics or the AlTiVCr matrix (Fig. 7). In the case of the as-cast sample, these two groups are not as clearly distinguished as in the heat-treated condition. Further analysis of the heat-treated condition indicated a matrix modulus of 194.7 ± 8.15 GPa and an intermetallic modulus of 241.2 ± 10.92 GPa. A comparison between the heat-treated AlTiVCr sample and the matrix of the heat-treated AlTiVCr-$Si_{7.2}$ reveals an increase in the Young's modulus of roughly 9 GPa between the two conditions. This effect was also captured by the DFT simulations which estimated the Young's modulus of the matrix phase to be 191.1 GPa (Fig. 6). In turn, the deviation between the computational and experimental results in terms of the Young's modulus of the matrix phase is less than 2%, and thus deemed highly reliable.

An additional important point is the effect the modification of the chemical composition of the matrix phase has on its elastic properties. As previously discussed, this modification occurs due to the formation of the Ti_5Si_3 intermetallic phase, thus depriving the AlTiVCr phase of Ti. There is an indication that this indirect manipulation of the chemical

composition of the matrix phase leads to elevated elastic properties. Cr has the highest specific shear and Young's moduli of all the metallic alloying elements [46], suggesting that the increased Young's modulus of this phase is due to the increased proportion of Cr contained within it.

A more significant difference (just over 10%) was observed in the nanoindentation measurements for Young's modulus between the as-cast condition (222.6 ± 35.6 GPa) and the heat-treated sample (201.2 ± 35.8 GPa). The microindentation results, however, produced a similar result for both of 205.4 ± 6.2 GPa in the as-cast and in the 203.5 ± 10.2 GPa heat-treated condition (Fig. 8). The measured density of the alloys was 5.07 $g.cm^{-3}$ and 4.97 $g.cm^{-3}$ for the AlTiVCr and AlTiVCr-Si_{72} respectively. In any case, the experimental measurements, and particularly those performed on the heat-treated sample, were once again in good agreement with the computational model. In turn, we calculated the specific Young's modulus of both the AlTiVCr and AlTiVCr-$Si_{7.2}$ alloys, using our experimental data for the density and E, as being 37.3 $GPa.cm^3.g^{-1}$ and 40.9 $GPa.cm^3.g^{-1}$ respectively, thus outperforming even the more advanced high modulus steels which range from 32 to 33 $GPa.cm^3.g^{-1}$ [3]. We believe that this manifestation of an elevated Young's modulus in the case of the AlTiVCr-$Si_{7.2}$ HEA is due to both the existence of the Ti_5Si_3 intermetallics and the indirect increase of the Cr content of the AlTiVCr matrix. This phenomenon could provide a novel concept for designing and fine-tuning the composition of high specific modulus HEAs. It is also evident that our computational approach is capable of successfully assessing the elastic properties of the tested alloys with reasonable accuracy. While this does not guarantee that similar success would be met were it applied to other multiphase materials, there is no fundamental barrier provided the required databases were available with appropriate accuracy. The results serve as a demonstration of feasibility and provide a pathway for elastic property prediction in novel multiphase HEA systems in the future.

4. Conclusions

We have presented our methodology for assessing novel multiphase materials through a multi-principle computational approach consisting of thermodynamic, *ab-initio* and homogenisation modelling coupled with experimental validation. We applied our methodology to the AlTiVCr and AlTiVCr-$Si_{7.2}$ high entropy alloys and managed to successfully estimate the elastic properties of both materials, yielding a deviation of 10% for the AlTiVCr alloy and only 2% for the AlTiVCr-$Si_{7.2}$ alloy. This is an important outcome, as in principle (given adequate thermodynamic databases and suitable choice of RVE for the relevant case) the applicability of the methodology is alloy-universal and solely depends on the accuracy of each individual modelling technique. Through this work, we have now identified the potential of both materials for further development and application within the field of lightweight, high specific modulus structural materials.

Supporting information

SupMat

Declaration of Competing Interest

The authors declare that they have no known competing financial interests or personal relationships that could have appeared to influence the work reported in this paper.

Acknowledgements

We would like to acknowledge EPSRC grant (EP/L016273) Centre for Doctoral Training in Advanced Metallic Systems and Volkswagen Group for supporting this research.

Via our membership of the UK's HEC Materials Chemistry Consortium, which is funded by EPSRC (EP/L000202, EP/R029431, EP/T022213), this work used the ARCHER UK National Supercomputing Service (http://www.archer.ac.uk).

We would also like to thank Mr. Neil Hind from the University of Sheffield for assisting in the design and execution of the heat treatment process and Ms. Eugenia Spiropoulou of ELKEME S.A for assisting us regarding the density measurements.

Supplementary materials

Supplementary material associated with this article can be found, in the online version, at doi:10.1016/j.mtla.2022.101365.

References

[1] European Environment AgencyTotal Greenhouse Gas Emission Trends and Projections in Europe, 2021 https://www.eea.europa.eu/data-and-maps/indicators/greenhouse-gas-emission-trends-7/assessment Accessed: 11/10/2021.
[2] M.F. Ashby, Materials Selection in Mechanical Design, 4th ed., Butterworth-Heinemann, 2010.
[3] H. Springer, C. Baron, A. Szczepaniak, V. Uhlenwinkel, D. Raabe, Stiff, light, strong and ductile: nano-structured high modulus steel, Sci. Rep. 7 (2017) 2757.
[4] F. Giustino, Materials Modelling Using Density Functional Theory, Properties and Predictions, 1st ed., Oxford University Press, Oxford, 2014.
[5] P. Hohenberg, W. Kohn, Inhomogeneous electron gas„ Phys. Rev. 136 (1964) 864–871.
[6] W. Kohn, L.J. Sham, Self-consistent equations including exchange and correlation effects, Phys. Rev. 140 (1965) 1133–1138.
[7] L. Vitos, Computational Quantum Mechanics for Materials, 1st ed., Springer-Verlag London Ltd, London, 2007.
[8] F. Tian, L.K. Varga, N. Chen, L. Delczeg, L. Vitos, Ab initio investigation of high-entropy alloys of 3d elements, Phys. Rev. B 87 (2013) 075144.
[9] F. Tian, L. Delczeg, N. Chen, L.K. Varga, J. Shen, L. Vitos, Structural stability of $NiCoFeCrAl_x$ high-entropy alloy from ab initio theory, Phys. Rev. B. 88 (2013) 085128.
[10] S. Huang, F. Tian, L. Vitos, Elasticity of high-entropy alloys from ab initio theory, J. Mat. Res. 33 (19) (2018) 2938–2953.
[11] A.J. Zaddach, C. Niu, C.C. Koch, D.L. Irving, Mechanical properties and stacking fault energies of NiFeCrCoMn high-entropy alloy, JOM 65 (12) (2013) 1780–1789.
[12] P. Cao, X. Ni, F. Tian, L.K. Varga, L. Vitos, Ab initio study of Al_xMoNbTiV high-entropy alloys, J. Phys.: Cond. Mat. 27 (2015) 075401.
[13] H. Ge, F. Tian, Y. Wang, Elastic and thermal properties of refractory high-entropy alloys from first-principles calculations, Comp. Mat. Sci. 128 (2017) 185–190.
[14] Y. Mu, H. Liu, X. Zhang, Y. Jiang, T. Dong, An ab initio and experimental studies of the structure, mechanical parameters and state density on the refractory high-entropy alloy systems, J. Alloys Comp. 714 (2017) 668–680.
[15] M. Liao, Y. Liu, L. Min, Z. Lai, T. Han, D. Yang, J. Zhu, Alloying effect on phase stability, elastic and thermodynamic properties of Nb-Ti-V-Zr high entropy alloy, Intermetallics 101 (2018) 152–164.
[16] L. Chen, X. Hao, Y. Wang, X. Zhang, H. Liu, First-principles calculation of the effect of Ti content on the structure and properties of TiVNbMo refractory high-entropy alloy, Mater. Res. Express 7 (2020) 106516.
[17] O.N. Senkov, J.M. Scott, S.V. Senkova, D.B. Miracle, C.F. Woodward, Microstructure and room temperature properties of a high-entropy TaNbHfZrTi alloy, J. Alloys Comp. 509 (2011) 6043–6048.
[18] O.N. Senkov, J.M. Scott, S.V. Senkova, F. Meisenkothen, D.B. Miracle, C.F. Woodward, Microstructure and elevated temperature properties of a refractory TaNbHfZrTi alloy, J. Mat. Sci. 47 (2012) 4062–4074.
[19] A. Kumar, M. Gupta, An insight into evolution of light weight high entropy alloys: a review, Metals (Basel) 6 (9) (2016) 199.
[20] O. Senkov, S.V. Senkova, C. Woodward, D.B. Miracle, Low-density, refractory multi-principal element alloys of the Cr–Nb–Ti–V–Zr system: microstructure and phase analysis, Acta Mat 61 (2013) 1545–1557.
[21] O. Senkov, S.V. Senkova, D.B. Miracle, C. Woodward, Mechanical properties of low–density, refractory multi-principal element alloys of the Cr–Nb–Ti–V–Zr system, Mat. Sci. Eng. A 565 (2013) 51–62.
[22] O.N. Senkov, S.L. Semiatin, Microstructure and properties of a refractory high-entropy alloy after cold working, J. Alloys Comp. 649 (2015) 1110–1123.
[23] B. Schuh, B Völker, J. Todt, N. Schell, L. Perrière, J. Li, J.P. Couzinié, A. Hohenwarter, Thermodynamic instability of a nanocrystalline, single-phase TiZrNbHfTa alloy and its impact on the mechanical properties, Acta Mat. 142 (2018) 201–212.
[24] N.D. Stepanov, N. Yu. Yurchenko, S.V. Zherebtsov, M.A. Tikhonovsky, G.A. Salishchev, Aging behavior of the HfNbTaTiZr high entropy alloy, Mat. Let. 211 (2018) 87–90.
[25] Y. Qiu, Y.J. Hu, A. Taylor, M.J. Styles, R.K.W. Marceau, A.V. Ceguerra, M.A. Gibson, Z.K. Liu, H.L. Fraser, N. Birbilis, A lightweight single-phase AlTiVCr compositionally complex alloy, Acta Mat. 123 (2017) 115–124.
[26] S. Huang, W. Li, O. Eriksson, L. Vitos, Chemical ordering controlled thermo-elasticity of $AlTiVCr_{1-x}Nb_x$ high-entropy alloys, Acta Mat. 199 (2020) 53–62.
[27] X. Huang, J. Miao, A.A. Luo, Lightweight AlCrTiV high-entropy alloys with dual-phase microstructure via microalloying, J. Mat. Sci. 54 (2019) 2271–2277.

[28] J.-O. Andersson, T. Helander, L. Höglund, P. Shi, B. Sundman, Thermo-Calc and DICTRA, computational tools for materials science, Calphad 26 (2) (2002) 273–312.
[29] S.J. Clark, M.D. Segall, C.J. Pickard, P. Hasnip, M.I.J. Probert, K. Refson, M.C. Payne, First principles methods using CASTEP, Z. Kristal. 220 (2005) 567–570.
[30] G.P. Francis, M.C. Payne, Finite basis set corrections to total energy pseudopotential calculations, J. Phys. Cond. Matter 2 (1990) 4395–4404.
[31] J. Perdew, K. Burke, M. Erzerhof, Generalized gradient approximation made simple, Phys. Rev. Let. 77 (1996) 3865–3868.
[32] P. Pulay, Convergence acceleration of iterative sequences. The case of SCF iteration, Chem. Phys. Let. 73 (2) (1980) 393–398.
[33] M. Verstraete, X. Gonze, Smearing scheme for finite-temperature electronic-structure calculations, Phys. Rev. B 65 (2001) 035111.
[34] J.D. Head, M.C. Zerner, A Broyden—Fletcher—Goldfarb—Shanno optimization procedure for molecular geometries, Chem. Phys. Let 122 (3) (1985) 264–270.
[35] H.J. Monkhorst, J.D. Pack, Special points for Brillouin-zone integrations, Phys. Rev. B 13 (12) (1976) 5188–5192.
[36] N.E. Koval, J.I. Juaristi, R.D. Muiño, M. Alducin, Elastic properties of the TiZrNbTaMo multi-principal element alloy studied from first principles, Intermetallics 106 (2019) 130–140.
[37] M.-M. Wu, L. Wen, B.-Y. Tang, L.-M. Peng, W.-J. Ding, First-principles study of elastic and electronic properties of MgZn2 and ScZn2 phases in Mg–Sc–Zn alloy, J. Alloys Comp. 506 (2010) 412–417.
[38] S.L. Omairey, P.D. Dunning, S. Sriramula, Development of an ABAQUS plugin tool for periodic RVE homogenisation, Eng. Comp. 35 (2019) 567–577.
[39] G.-D. Cheng, Y.-W. Cai, L. Xu, Novel implementation of homogenization method to predict effective properties of periodic materials, Acta Mech. Sin. 29 (2013) 550–556.
[40] P.F. Zhang, Y.X. Li, P.K. Bai, First principles study of Ti_5Si_3 intermetallic compounds with Cu additions: elastic properties and electronic structure, IOP Conf. Ser.: Mat. Sci. Eng. 284 (2017) 012013.
[41] H.-Y. Wang, W.-P. Si, S.-L. Li, N. Zhang, Q.-C. Jiang, First-principles study of the structural and elastic properties of Ti5Si3 with substitutions Zr, V, Nb, and Cr, J. Mat. Res. 25 (12) (2010) 2317–2324.
[42] D.V. Louzguine, A. Inoue, Crystallization behaviour of $Ti_{50}Ni_{25}Cu_{25}$ amorphous alloy, J. Mat. Sci. 35 (2000) 4159–4164.
[43] F. Anselin, Etude de la decomposition de la phase γdans le ternaire uranium-plutonium-molybdene (20), in: Proc. Int. Conf. Plutonium Metall. 2nd, 1961, pp. 367–384.
[44] R. Ray, B.C. Giessen, N.J. Grant, The constitution of metastable titanium-rich Ti-Fe alloys: an order-disorder transition, Metall. Trans. 3 (1972) 627.
[45] Natl. Bur. Stand. (U.S.), Standard X-ray diffraction powder patterns, Circ. 539 (8) (1958) 64.
[46] WebElements, The periodic table of the elements, https://www.webelements.com, Accessed 11/10/2021.